ADVANCED FUNCTIONAL MATERIALS
www.afm-journal.de

Initial Growth Mode, Nanostructure, and Molecular Stacking of a ZnPc:C60 Bulk Heterojunction

Hyo Jung Kim, Ji Whan Kim, Hyun Hwi Lee,* Byeongdu Lee, and Jang-Joo Kim**

The initial growth modes of ZnPc films is examined, revealing the previously undescribed nanoscale crystal structure evolution and the nanograins of the ZnPc:C60 mixed layers in the thin films. Initially, the ZnPc molecules are stacked in the preferred γ(200) configuration, similar to the structures of CuPc. The ZnPc thin film growth display 2D planar to 3D island growth after the initial compressive strain had relaxed in films 7–8 MLs thick. 3D island formation decreases the prevalence of the preferred ordering in the γ(200) crystals. The ZnPc films consist of randomly distributed ellipsoid nanograins during the initial growth stages. The ellipsoid nanograins transition to an ordered state later in the growth process. Insertion of C60 changes the preferred molecular stacking of ZnPc, and β(100) forms in the ZnPc:C60 layers fabricated at room temperature, which is usually observed at high annealing temperatures (200 °C) in a single ZnPc film. The ellipsoid ZnPc nanograins also retain their shapes in the ZnPc:C60 mixed layers. The formation of β(100) and the presence of ellipsoid nanograins in the mixed layer are related to improvements relative to planar devices in the organic photovoltaic device performance.

1. Introduction

Formation of bulk heterojunctions (BHJs) between donor and acceptor molecules is a way to maximize the optical absorption length while accommodating the short exciton diffusion length in organic thin films. These efforts have been particularly successful in the area of solution-processed polymer organic photovoltaics (OPVs).[1–3] Thermally deposited small molecular (SM) OPVs have also used BHJs to improve device performance relative to planar-heterojunction type devices.[4–7] Generally, BHJs in thermally deposited SM OPVs are fabricated via the co-deposition of donor and acceptor materials and large effort has been devoted to improving BHJs with the goal of creating interpenetrating networks.

Formation of BHJ during co-deposition relies on the initial growth mode and relative magnitude of the interaction energy between like molecules and between unlike molecules.[5] At the initial growth regime, the strain generally relaxes to transform from the surface structure to its bulk structure within 1 ~ 5 monolayers and the initial growth mode dictates the further growth.[8,9] If the interaction energy between like molecules is larger than that between unlike molecules, similar molecules tend to aggregate, and BHJs form during co-deposition or modified thermal deposition, with nanoscale structures. The CuPc:C60 system satisfies the requirement, where the interaction energies between nearest neighbors are 0.87 eV (CuPc–CuPc), 1.5 eV (C60–C60), and 0.44 eV (CuPc–C60).[10] ZnPc and CuPc are planar type phthalocyanine molecules, which have a herringbone structure and stack with a γ(200)[11–13] preferred orientation in thin films (less than 50 nm thick) during thermal evaporation. Due to the similar molecular shape and crystal structure, ZnPc and CuPc are considered to have similar initial growth mode. In addition, ZnPc and CuPc are similar in energy levels. Therefore, the ZnPc:C60 system is expected to behave similarly during the codeposition of the consisting molecules.

Despite of the similarities in the molecular structure and the molecular staking in the crystal, we show in this paper that ZnPc and CuPc films are significantly different in their initial growth state based on GISAXS and GIWAXS analysis. The ZnPc:C60 nanostructures were also examined using GISAXS and GIWAXS to find different nanostructures in this system. The ZnPc:C60 nanostructure was found to be related to larger improvement of the solar cell performance in BHJ structures compared to planar-heterojunction structures than the CuPc:C60 system.

2. Results and Discussion

Figure 1a,b display the GIWAXS images of the 5 nm and 50 nm thick ZnPc and CuPc films grown on silicon wafers, respectively. The images clearly show the strong (200) diffraction peaks in the vertical direction, indicating that the ZnPc and CuPc films have preferred orientation with edge-on arrangement of the

Dr. H. J. Kim, J. W. Kim, Prof. J.-J. Kim
Department of Materials Science and Engineering and OLED Center
Seoul National University
Seoul 151-744, Republic of Korea
E-mail: hjkim08@snu.ac.kr; jjkim@snu.ac.kr
Dr. H. H. Lee
Pohang Accelerator Laboratory, POSTECH
Pohang, Gyungbuk 790-784, Republic of Korea
E-mail: hhleec@postech.ac.kr
Dr. B. Lee
X-ray Science Division
Argonne National Laboratory
Argonne, IL 60439 USA

DOI: 10.1002/adfm.201200778

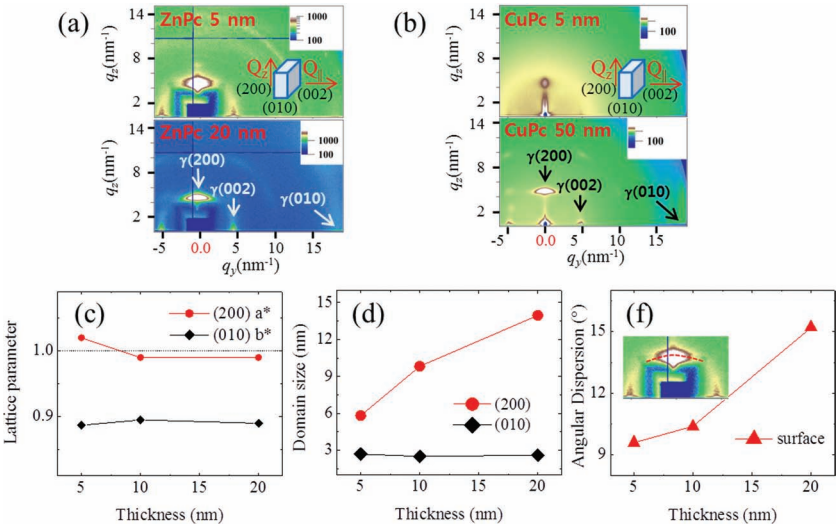

Figure 1. a,b) GIWAXS 2D images of the ZnPc and CuPc films for 5 nm and 50 nm thick films, respectively. c) The normalized lattice parameters, d) crystal domain size, and af) ngular dispersion of the γ-phase ZnPc as a function of the film thickness. The angular dispersion indicates the FWHM of the γ(200) peak in the circular direction, as shown in the dotted line in the inset of (e). The peak positions of the (200), (002), and (010) orientations of the γ-phase are shown in the GIWAXS 2D diffraction images.

molecules (monoclinic (C2/n) γ(200) arrangements), consistent with the previous reports.[8,13] The (010) and (002) peaks are observed along the horizontal direction in the GIWAXS images as expected. The monoclinic γ-phase is sometimes described as the α-II phase in literature, although we use the notation "γ-phase" here, in accordance with recent reports of the crystal structures.[12,13] Detailed information about the ZnPc crystals in the film were obtained by analysis of the GIWAXS images. The analysis results are shown in Figure 1c–e, which show, respectively, the lattice parameters (Figure 1c), crystal domain size (Figure 1d), and angular spread of orientation of the ZnPc crystals (Figure 1e) in the films with different thicknesses. The lattice parameters a^* and b^* in Figure 1c are the normalized lattice parameters of the ZnPc films to those of the γ-phase CuPc crystal whose parameters are a_0 = 2.633 nm, b_0 = 0.381 nm, and c_0 = 2.371 nm, and the β angle is 94.3°.[13] The crystallographic detail information of the γ-phase ZnPc crystal has not been reported yet. K. Leo's group adopted γ-phase CuPc unit cell for γ-phase ZnPc. The lattice parameters of the 5 nm thick ZnPc film in Figure 1c show that the lattice parameter a is larger than the bulk value and the lattice parameter b is smaller than the bulk value, indicating that the ZnPc film at the initial growth region is under compressive stress in the lateral direction. The lattice parameter a decreased, whereas the lattice parameter b increased at the thickness of 10 nm, impying that the compressive stain relaxed at thicknesses exceeding 10 nm. Still it is curious that both a^* and b^* are all smaller than 1. This may come from the uncertainty of the lattice parameters of the γ-phase ZnPc crystals. The changes in the lattice parameters can also be related to the variation of the tilt angle of the molecules because the tilt angle and the molecular conformation may also change during the growth.[14] The tilt of the organic molecules is related to the interaction energy between organic molecule and the substrate. The relaxed lattice parameter in the thin film should be measured to clarify the issue. The angular spread of the ZnPc films, which is related to the variation of the orientation among the crystals, increased with the film thickness as shown in Figure 1e. In contrast, our previous report[8] showed that the angular spread of the CuPc films did not increase with increasing the film thickness up to the thickness of 50 nm, and no strain relaxation was observed even in the 50 nm thick films. We also showed that an ultrathin (5 nm) CuPc layer consisted of regularly ordered disc-type CuPc grains and the ordering was retained up to the CuPc film thickness of 50 nm.

The initial growth mode of the ZnPc layer was analyzed using the GISAXS images shown in **Figure 2**a–c for different

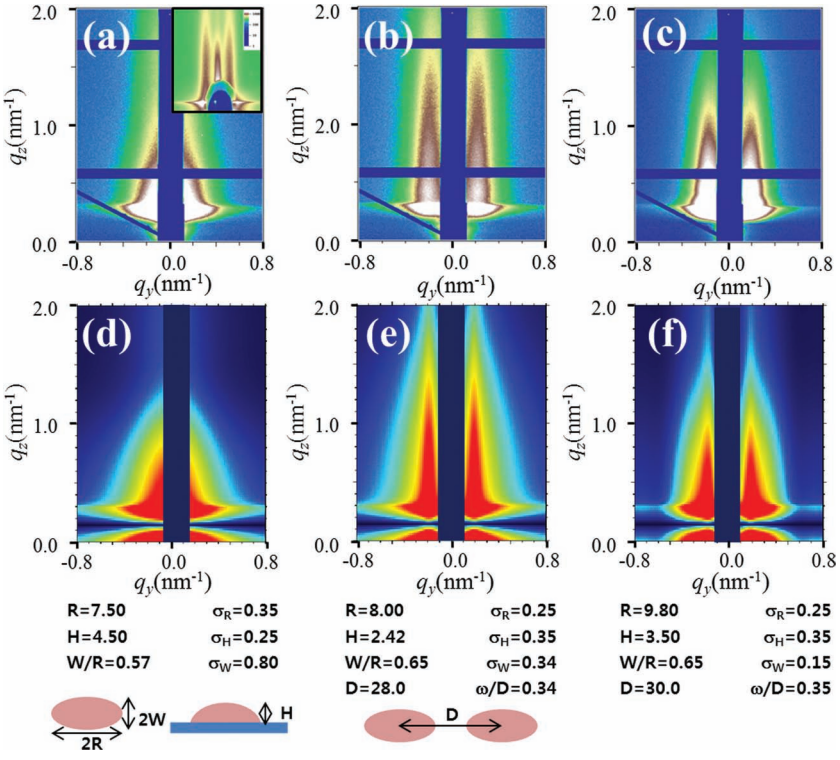

Figure 2. a–c) GISAXS images and d–f) IsGISAXS calculation results for 5 nm, 10 nm, and 20 nm thick ZnPc films. The inset of (a) shows the GISAXS image of a 5 nm thick CuPc film. The calculation is based on the ellipsoid nanograins, as described in the schematic diagram.

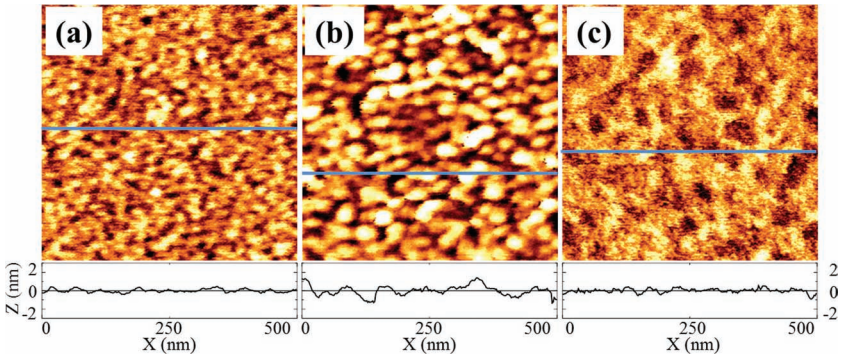

Figure 3. a,b) AFM images of 5 nm (σ_{rms} = 0.18 nm) and 20 nm (σ_{rms} = 0.65 nm) thick ZnPc films, respectively. c) An AFM image of a ZnPc:C_{60} (20 nm, σ_{rms} = 0.21 nm) mixed film.

thicknesses. The GISAXS image of the 5 nm thick CuPc film was inserted as the inset of the Figure 2a for comparison, which can be modeled using the regularly ordered disc-type CuPc grains. In contrast to the CuPc film, the 5 nm thick ZnPc film did not reveal a structure factor. The structure factor was apparent in the 10 nm thick ZnPc film, and the shape and regular distribution was retained in the 20 nm thick film as shown in Figure 2b,c. The GISAXS images were used to model the structure of the films using the IsGISAXS.[15] The images were modeled very well using ellipsoid-shaped nano-grains as shown in Figure 2d–f for the 5 nm, 10 nm, and 20 nm thick ZnPc films, respectively. In the calculation, R, W, and H are the radius, the width, and the height of an ellipsoid, as described in the schematic diagram shown in Figure 2. σ_R, σ_H, and σ_W represent the standard deviation of the radius, width, and height. D and ω/D are the average distance between ellipsoids and their distribution, respectively. The 5 nm thick ZnPc thin film consisted of irregularly arranged ellipsoid-shaped ZnPc nanograins (Figure 2d), but they became ordered at the thickness of 10 nm, and this ordering was retained in the thicker layer.

Figure 3a–c show the atomic force microscopy (AFM) images of the ZnPc and ZnPc:C60 films. The surface of the 5 nm thick ZnPc film was smooth with a root mean square roughness of ≈0.18 nm (Figure 3a). The smooth surface changed to a rough one with tens of nanometer sized islands as the thickness increases to 20 nm. The morphological changes from smooth surface to rough one indicates that the ZnPc films grow according to the Stranski–Krastanov (S–K) growth mode, in which 2D layer-by-layer growth transformed to a 3D island growth mode. This transition to the S–K growth mode was most frequently observed in the quasi-epitaxial growth of organic molecules.[9] In the S–K growth mode, the lattice mismatch between the film and the substrate relaxes within 1–5 molecular layers (MLs), resulting in a rough columnar surface. The 5 nm thick ZnPc film includes a 4 ML stacking under compressive strain. This strain relaxed at the thickness exceeding 10 nm, corresponding to a molecular stacking structure of 8 MLs. Therefore, the S–K growth mode in the ZnPc films where the transition from the 2D layer-by-layer growth to regular 3D islands takes place during the growth must be related to the strain relaxation.

The smooth surface of the 5 nm thick ZnPc films seems to contradict the GISAXS results which showed that the film consisted of elliptic nanograins. However, the smooth surface of the film does not necessarily mean the film is homogeneous. In our previous paper describing ultrathin (5 nm) CuPc films, the surface morphology was very flat in the AFM images.[8] Despite the flat surface, which resulted from the planar growth, the GISAXS images showed disc-type nanograins, as shown in the inset of Figure 2a, with clearly separated SAXS wings. Flat layers are not generally related to nanograins in inorganic systems; however, the flat surface morphology of the phthalocyanine films differed from the flat surface morphology of inorganic films. A film consisting of nanograins included less packed low-density regions (or gaps). If the regions had a smooth surface, an AFM topographical image may not have been able to distinguish these regions from the nanograins.

Co-deposition of C60 with ZnPc does not influence the structure of the ZnPc films when the film is thin. However, it has a significant influence on the resulting morphologies for thick films. First of all, three-dimensional islands were not observed in the AFM measurements of a 20 nm thick ZnPc:C60 mixed layer (as shown in Figure 3c. The incorporation of C60 favored the formation of smooth surfaces and the roughness of ZnPc:C60 films was similar to that of the 5 nm thick ZnPc films. Secondly, GISAXS measurements in **Figure 4**a,b and the simulation of the nanostructures in Figure 4c and d show that the nanostructure of the 5 and 20 nm thick ZnPc:C60 films are also similar to that of the 5 nm thick ZnPc film, indicating that

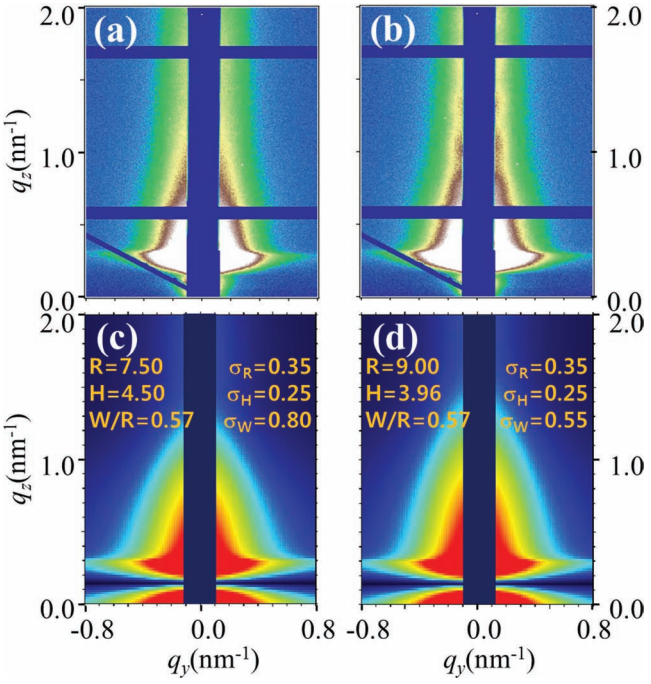

Figure 4. a,b) GISAXS images of 5 nm and 20 nm thick ZnPc:C_{60} mixed layers. c,d) The IsGISAXS calculation results based on the ellipsoid nanograin model.

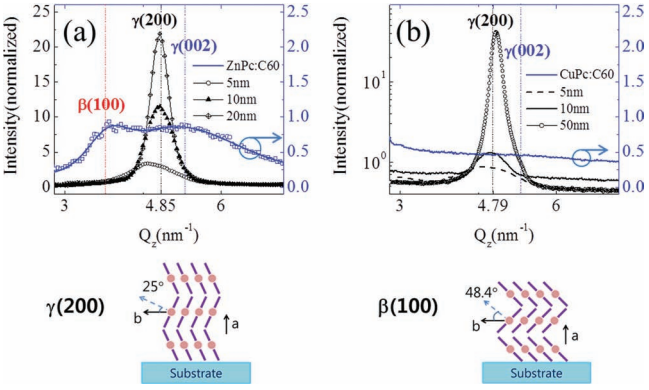

Figure 5. a) The γ(200) ZnPc peak (Q_z = 4.85 nm^{-1}) for 5 nm, 10 nm, and 20 nm thick films. The mixed ZnPc:C_{60} layer displayed two peaks corresponding to the β(100) and γ(002) configurations. The average sizes of the β(100) and γ(002) configurations were 7.8 nm and 2.3 nm, respectively. b) The γ(200) CuPc peak (Q_z = 4.79 nm^{-1}) at 5 nm, 10 nm, and 50 nm films. No clear diffraction peaks were observed from the mixed layer, as indicated by the blue line in (b). The schematic diagram shows the molecular stacking of the γ and β phases in ZnPc crystals aligned along the *a*-axis on the substrate.

the ellipsoid ZnPc nanograins are formed at the initial stages of the film growth and are retained in the 20 nm thick ZnPc:C60 mixed layer without experiencing the transition from the 2D to 3D growth.

Thirdly, the insertion of C60 changed the crystal structure of ZnPc nano grains from γ phase to the mixture of γ phase and β phase[16] with the preferred orientations of γ(200) and β(100), respectively, as displayed in **Figure 5**. The average crystal sizes of the β(100) and γ(002) phases were 7.8 nm and 2.3 nm, respectively. The β-phase is only observed by high-temperature annealing of pure ZnPc films at temperatures above 200 °C. In this work, the mixed layer was fabricated at RT. It is unclear now why C60 induces the formation of the β-phase, but this effect may be related to the interaction energy between C60 and the ZnPc molecules. It is interesting to note that the β-phase was not observed in the CuPc:C60 mixed layer, as shown in Figure 5b. The only difference between ZnPc:C60 and CuPc:C60 was the interaction energy with C60. As mentioned previously, the CuPc–C60 interaction energy was 0.44 eV. Until now, the ZnPc–C60 interaction energy was thought to be similar to that of CuPc–C60, but no evidence has been brought forth to clearly support this hypothesis. Our results suggest that C60 behaves differently in the contexts of the ZnPc:C60 and CuPc:C60 systems. Further studies of the interaction energy and crystal formation are needed.

The molecular stacking of the γ and β phases are illustrated in Figure 5. The main difference between the γ and β phases is the angle between the *b* axis and the vector normal to the M-N bonds. This angle is 25°–28° in the γ-phase and 48.4° in the β-phase. A comparison with γ(200) revealed that more molecules were present lying on the substrate in the β(100) configuration, as shown in the schematic diagram. The molecular dipole moment in phthalocyanine molecules is parallel to the molecular plane. As a result, more dipoles are lying down in the β(100) configuration than in the γ(200) configuration. The recumbent dipoles increase the absorption cross-section due to alignment between the dipole and the angle of light polarization. The β-phase, which was preferentially aligned along the <100> direction, provided a good absorption cross-section in organic photovoltaic devices.

Planar heterojunction (PHJ) and BHJ devices were fabricated in the following configurations: PHJ OPV [ITO/ZnPc (20 nm)/C_{60} (40 nm)/BCP (8 nm)/Al (100 nm)] and a co-deposited BHJ OPV device [ITO/ZnPc (3 nm)/co-deposited ZnPc:C_{60} (40 nm)/C_{60} (10 nm)/BCP (8 nm)/Al (100 nm)]. The co-deposited BHJ device displayed a significantly higher J_{sc} compared to the PHJ device, 9.16(±0.04) as compared to 5.37(±0.04) mA cm^{-2}, respectively, because the large number of interfaces facilitated charge separation by co-deposition. As a result, the power conversion efficiency (PCE) improved to 1.71(±0.02)% relative to the PHJ (1.43 ± 0.08%) device, which is consistent to K. Leo group's result.[10] In the BHJ and PHJ devices, the FFs were 0.38(±0.01) and 0.53(±0.01), respectively.

3. Conclusion

The initial stages of ZnPc film growth were investigated. The ZnPc film growth proceeded along the S–K growth mode in that growth transitioned from an initial 2D planar growth mode to 3D island formation. This transition was related to the strain relaxation. The initial compressive strain relaxed in films around 10 nm thick (8 MLs). Relaxation induced formation of 3D islands and a sparse distribution of the preferred orientations of ZnPc crystals. The insertion of C60 induced stacking among ZnPc molecules in the β(100) and γ(002) configurations, producing very flat surfaces. The formation of a β-phase with a (100) orientation yielded a higher absorption cross-section than the γ(200) configuration because the ZnPc dipoles were aligned along the direction of light polarization in the OPV devices. The presence of a range of nanograin sizes in the β(001) configuration (7.8 nm) and the γ(002) configuration (2.3 nm) improved the performance of BHJs containing C60 because the grains packed in the film more densely than did monodisperse grains. The presence of C60 did not affect the formation of ellipsoid ZnPc nanograins during the initial stages of growth; however, it affected the regular arrangement of nanograins during the later stages. A size assessment revealed that the ellipsoids observed in the GISAXS results appeared to be related to the γ(002) configuration.

4. Experimental Section

Sample Preparation: ZnPc was purchased from Aldrich and purified two times with sublimation. C_{60} was purchased from SES Research. ZnPc and ZnPc:C_{60} films were prepared by thermal evaporation under a vacuum of 10^{-7} Torr on Piranha (H_2SO_4:H_2O_2 = 4:1 mixed solution) treated Si substrates for X-ray measurements. The film thickness was monitored by thickness monitor equipped in the evaporation chamber.

X-Ray Measurements: GISAXS (grazing incidence small-angle X-ray scattering) and GIWAXS (grazing incidence wide-angle X-ray scattering) measurements were performed at the 12ID-B and 12ID-C beam lines of the Advanced Photon Source (APS) at the Argonne National Laboratory.

The X-ray energy was 12 keV. The distance from the sample to the detector was 1994.6 mm for GISAXS, while it was 227 mm for GIWAXS measurements, respectively. A PILATUS 2M detector was used for both measurements. GISAXS and GIWAXS were all measured at the incidence angle of 0.13°, which is higher than 0.124° (calculated with a mass density of 1.62 g cm^{-3} for the crystalline monoclinic γ-ZnPc structure[13]) the critical angle of ZnPc in 12 keV.

Device Fabrication and Characterization: The ITO-coated glass substrates were cleaned with acetone and isopropyl alcohol. The substrates were exposed to UV–O_3 for 10 min prior to use. ZnPc, C_{60}, 2,9-dimethyl-4,7-dipheyl-1,10-phenanthroline (BCP), and Al were thermally deposited under a vacuum of 10^{-7} Torr. Each layer was successively evaporated without breaking the vacuum, and all devices were flushed with N_2 prior to the photocurrent measurements. The photocurrents were measured under illumination from an AM1.5 solar simulator (300W Oriel 91160A). The light intensity was carefully calibrated using a standard silicon solar cell (NREL). A Keithley 237 source measurement unit was used for current density–voltage characteristics.

Acknowledgements

This research was supported by Basic Science Research Program through the National Research Foundation of Korea(NRF) funded by the Ministry of Education, Science and Technology (R15-2008-006-01001-0) and the New & Renewable Energy Technology Development Program of the Korea Institute of Energy Technology Evaluation and Planning(KETEP) grant funded by the Korea government Ministry of Knowledge Economy (No. 20113020010070). This work was also supported by PAL through the abroad beamtime program of Synchrotron Radiation Facility Project under MEST. Use of the Advanced Photon Source, an Office of Science User Facility operated for the U.S. Department of Energy (DOE) Office of Science by Argonne National Laboratory, was supported by the U.S. DOE under Contract No. DE-AC02-06CH11357.

Received: March 20, 2012
Published online: June 13, 2012

[1] X. Yang, J. Loos, S. C. Veenstra, J. H. Verhees, M. M. Wienk, J. M. Kroon, M. A. J. Michels, R. A. J. Janseen, *Nano Lett.* **2005**, *4*, 579.
[2] W. Ma, C. Yang, X. Gong, K. Lee, A. J. Heeger, *Adv. Funct. Mater.* **2005**, *15*, 1617.
[3] G. Dennler, C. Ssharber, C. J. Brabec, *Adv. Mater.* **2009**, *21*, 1323.
[4] P. Peumans, S. Uchida, S. R. Forrest, *Nature* **2003**, *425*, 158.
[5] F. Yang, K. Sun, S. R. Forrest, *Adv. Mater.* **2007**, *19*, 4166.
[6] H. X. Wei, J. Li, Z. Q. Xu, Y. Cai, J. X. Tang, Y. Q. Li, *Appl. Phys. Lett.* **2010**, *97*, 083302.
[7] J. W. Kim, H. J. Kim, H. H. Lee, T. Kim, J.-J. Kim, *Adv. Funct. Mater.* **2011**, *21*, 2067.
[8] H. J. Kim, J. W. Kim, H. H. Lee, T.-M. Kim, J.-J. Kim, *J. Phys. Chem. Lett.* **2011**, *2*, 1710.
[9] S. R. Forrest, *Chem. Rev.* **1997**, *97*, 1793.
[10] S. Pfuetzner, J. Meiss, A. Petrich, M. Riede, K. Leo, *Appl. Phys. Lett.* **2009**, *94*, 253303.
[11] C. J. Brown, *J. Chem. Soc. A* **1968**, 2488.
[12] P. Erk, H. Hengelsbeg, M. F. Haddow, R. v. Gelder, *CrystEngComm* **2004**, *6*, 474.
[13] C. Schünemann, C. Elschner, A. A. Levin, M. Levichkova, K. Leo, M. Riede, *Thin Solid Films* **2011**, *519*, 3939.
[14] S. Kowarik, A. Gerlach, F. Schreiber, *J. Phys.:Condens. Matter* **2008**, *20*, 184005.
[15] R. Lazzari, *J. Appl. Cryst.* **2002**, *35*, 406.
[16] W. R. Scheidt, W. Dow, *J. Am. Chem. Soc.* **1997**, *99*, 1101.